communications materials

ARTICLE

https://doi.org/10.1038/s43246-023-00393-0 OPEN

Boosting inhibition performance of natural polyphenols for the prevention of calcium oxalate kidney stones through synergistic cooperativity

Si Li[1], Donghui Zhou[2], Zuoxuan Zhu[1,3], Xiaoyue Tan[2], Weiwei Tang[1,3]✉ & Junbo Gong[1,3]✉

Binary drug combination usually targets different pathways to achieve cooperative therapy, but the exploitation of synergistic cooperativity between crystal growth modifiers that bind to the same site for preventing pathological biomineralization has yet to be realized. Here, we report that the binary inhibitor combinations of citrate with natural polyphenols can boost the inhibitory efficacy of calcium oxalate monohydrate crystallization, a primary component of kidney stones, up to four-fold greater than citrate alone. A combination of experimental and simulation techniques shows a strong synergy of four citrate-polyphenol inhibitor pairs on suppressing calcium oxalate monohydrate growth with minimal amounts of inhibitor, resulting from the reduction of growth kinetic constant paralleled with suppressing the crystallization driving force. Further, the inhibitor pairs demonstrated both in vitro and in vivo synergistic reductions of crystal-cell interactions, renal calcium oxalate deposition, and kidney injury, collectively presenting an effective therapeutic strategy for preventing calcium oxalate stones by boosting the inhibition efficacy of potent inhibitor pairs.

[1] School of Chemical Engineering and Technology, State Key Laboratory of Chemical Engineering, The Co-Innovation Center of Chemistry and Chemical Engineering of Tianjin, Tianjin University, Tianjin 300072, China. [2] School of Medicine, State Key Laboratory of Medicinal Chemical Biology, Nankai University, Tianjin 300071, China. [3] Haihe Laboratory of Sustainable Chemical Transformations, Tianjin 300192, China. ✉email: wwtang@tju.edu.cn; junbo_gong@tju.edu.cn

Pathological biomineralization is an undesirable crystallization process associated with human diseases[1–5]. Calcium oxalate (CaC_2O_4, CaOx) is one of the most common biominerals in nature[6], but its mineralization in humans leads to the formation of deadly kidney stones that affect approximately 10% of the world population with increasing prevalence[7–9]. Besides, stone formers are at risk of hypertension[10], chronic kidney disease[11,12], and end-stage renal disease[8]. The formation of CaOx stones is a consequence of excessive urinary CaOx supersaturation occurring in acquired metabolic defects, genetic disease, or dietary and lifestyle factors[8,13,14]. Subsequently, crystals adhere directly to the renal epithelium or Randall's plaques[13,15], forming a nidus for further growth and aggregation with urinary compositions, developing into centimeter-size stones[13,16]. Although CaOx has three reported hydrated phases including calcium oxalate monohydrate (COM), calcium oxalate dihydrate, and calcium oxalate trihydrate, the thermodynamically most stable form, COM, is most commonly seen in kidney stones[5].

Current treatments of kidney stones have gained advances in surgical management, e.g. shock-wave lithotripsy, and endoscopic technology[8,17,18]. This short-term management can alleviate renal colic induced by stones through stone removal[8], but the patients regain kidney stones after surgery with a relapse rate as high as over 50% within 5–10 years[19,20]. The current clinic puts great attention on the long-term medical management of nephrolithiasis through dietary modification and/or pharmacological treatment to alter urinary chemistry[21], which is designed to decrease the renal CaOx crystallization and crystal-cell interactions, thereby reducing stone formation. It is recognized that understanding the inhibitory effects of (bio)molecules in urine and extrinsic potent drugs on COM biomineralization is one of the most pivotal issues relevant to the treatment of kidney stone disease[3,8,9,21].

Accordingly, many in vitro studies worked with crystal growth inhibitors, ranging from urinary ions to proteins, have mainly focused on assessing the inhibition efficacy on bulk crystallization and crystal growth of COM, as well as inhibitory mechanisms[22–25]. Some metal ions (e.g. Zn^{2+})[24], citrate derivatives[9], polyphosphates[16], and urinary proteins containing carboxyl, sulfate, hydroxyl, or phosphate functional groups were suggested as the potent inhibitor drug candidates for preventing the formation of kidney stones[22,26] Citrate (CA), one of the urinary constituents, was shown to suppress renal CaOx crystallization and crystal-cell interactions[5,9,27,28]. Rimer et al. [29] found hydroxy-citrate as a crystallization inhibitor to retard COM growth by a unique strain-induced dissolution mechanism. Apart from carboxylic acid molecules, our previous study reported natural polyphenols as a new type of inhibitor on COM crystallization. Recent studies have established that COM crystal growth follows the classical spiral growth, whereby steps on the crystal surface advance by incorporation of solutes[3,30]. DeYoreo et al. [31] identified the polypeptide, $(DDDS)_6DDD$, functioning as a step pinner to impede step propagations, whereas $(DDDG)_6DDD$ is a kink blocker that frustrates solutes' incorporation into kinks. Step pinner molecules adsorbed on the terrace of crystal surfaces reduce the rate of step growth by imposing a surface tension on the advancing layer when two adsorbed species are separated by a distance smaller than the critical radius of the curved step and thereby decreasing local supersaturation[32]. CA was found to function as a combined role of step pinning and kink blocking[33]. We showed that gallic acid (GaA) and protocatechuic acid (PrA) are a step pinner and a kink blocker, respectively (Fig. 1a and see Supplementary Discussion 1), whereas ellagic acid (EA) and pyrogallic acid (PGA) function as dual inhibitor of step pinner and kink blocker, resembling citrate.

Studies on CaOx crystallization uncovered inhibitors that are more effective than the current therapies[26], but the action concentration of a single inhibitor to completely suppress crystallization is high with noticeable toxicity. A more effective strategy to increase inhibition efficacy with a low dose is thus desired, e.g. the use of binary inhibitor combinations that are common in many drug formulations for a wide range of diseases[34–37]. However, the combination of inhibitor (bio)molecules is capable of producing synergistic, additive, or even antagonistic effects[37,38]. It was found that the combined use of CA with chondroitin sulfate leads to a synergistic effect on COM growth suppression[39], but another study reported the strong antagonistic cooperativity between inhibitor pairs[37]. Furthermore, the fundamental mechanism of cooperative action between growth inhibitors remains elusive and is crucial for designing and developing a new formulation of drug combinations to boost the suppression performance of kidney stone formation.

Herein, we pair CA with natural polyphenols (i.e., GaA, EA, PGA, or PrA) to examine the effect of their cooperativity on COM crystallization and to address the underlying molecular mechanism of inhibitory action. The binary inhibitor combinations were selected as CA (step pinner and kink blocker) with EA (step pinner and kink blocker), PGA (step pinner and kink blocker), GaA (step pinner), and PrA (kink blocker), as discussed in Supplementary Discussion 1 and Supplementary Figs. 4–7. We observed more than 400% enhanced inhibition performance of inhibitor pairs on COM crystallization than CA alone with minute amounts of inhibitor. This unexpectedly strong synergistic cooperativity of inhibitor pairs was unveiled by a combination of in situ atomic force microscopy (AFM) and simulation techniques. Our results also demonstrate that these inhibitor combinations are able to synergistically diminish crystal-cell interactions that exhibit an enhanced reduction of the number of adhered crystals accompanied by increasing cell viability. Moreover, the in-vivo proof-of-concept study of a CaOx-induce nephrocalcinosis mouse model shows synergy in reductions of renal CaOx deposition and kidney injury using combinations of CA/PGA, CA/EA, and CA/GaA. Collectively, these findings provide an effective therapeutic approach for preventing CaOx-related kidney stones via boosting inhibition efficacy with synergistic cooperativity of binary inhibitor combinations.

Results

Synergistic cooperativity of binary inhibitors on CaOx crystallization. Bulk crystallization was performed at pH 6.4 ± 0.4, a physiological pH range of urine for kidney stone formation[9,40], to evaluate the effects of inhibitor pairs on calcium oxalate monohydrate (COM) crystallization. Figure 1b shows SEM images of COM crystals obtained in the presence of binary inhibitors that display significant changes in shape and dimension. The habit of COM crystals generate in pure solutions shows a pseudohexagonal shape bounded with $(12\bar{1})$, (021), and (010) facets and the elongated growth along [001] direction (Fig. 1b, control). CA imposes the growth impedance on the apical tips of COM crystals in the *c*-axis and produces the octagonal-shaped crystal (Fig. 1b, CA). In contrast, EA binds to COM (021) and $(12\bar{1})$ surfaces, decreasing the thickness and aspect ratio of crystals (Supplementary Fig. 1). The combination of CA/EA pairs produces flaky and octagonal-shaped COM crystals, indicating the synergistic cooperativity of these two inhibitors on COM growth suppression (Fig. 1b, CA & EA). The similarly synergistic growth inhibition behavior on COM crystals was also seen in other inhibitor pairs of CA/GaA, CA/PrA, and CA/PGA wherein their produced crystal morphologies display the combined binding specificity of individual inhibitors (Fig. 1b and Supplementary Fig. 8). The enhanced reduction of [001]/[010] aspect ratio (Fig. 1c) further appears to confirm the synergy of inhibition activity. COM

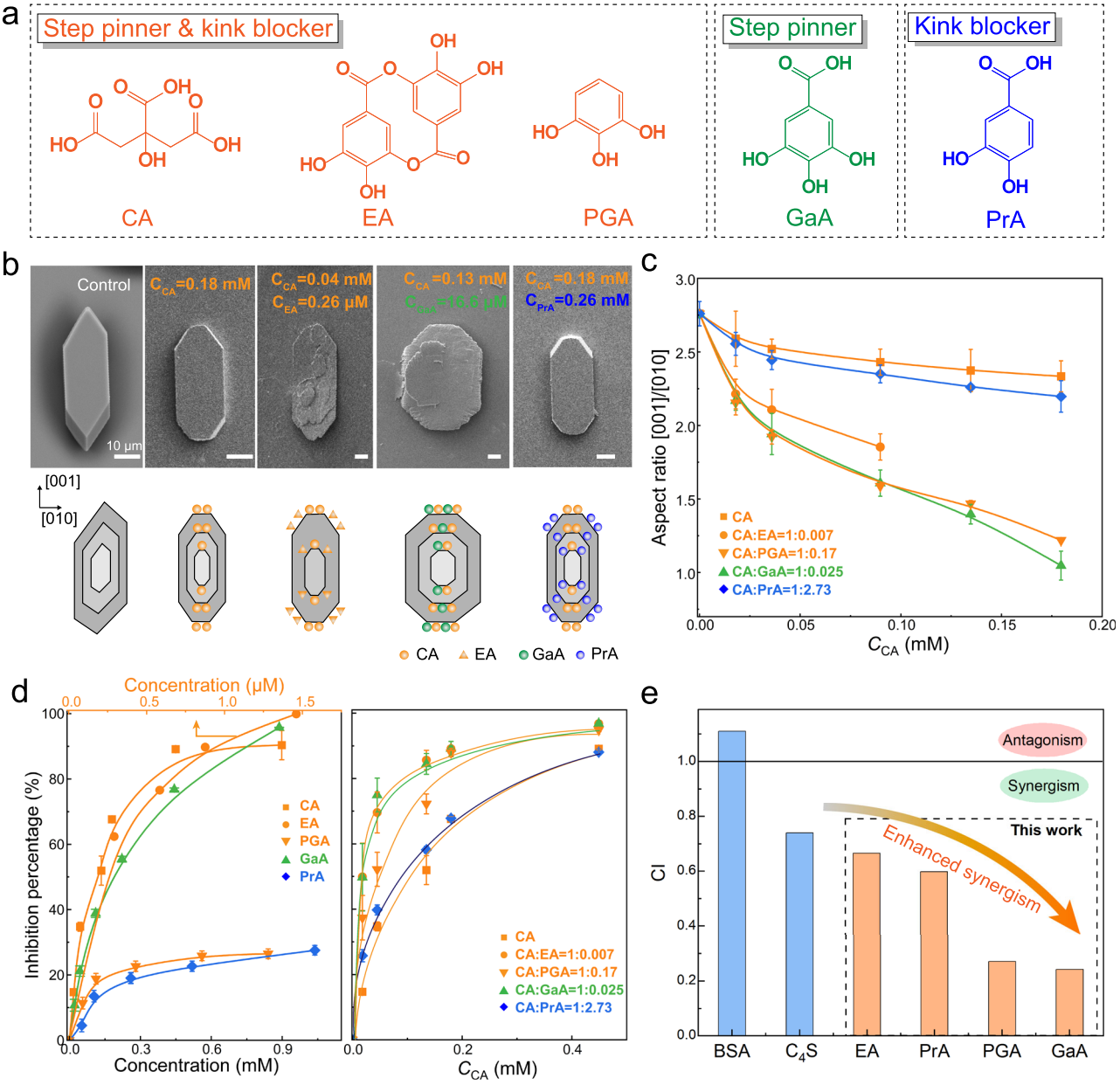

Fig. 1 Synergistic cooperativity of inhibitor pairs on suppressing bulk growth of COM crystals. a Molecular structures of step pinner and kink blockers (CA, EA, PGA), step pinner (GaA), and kink blocker (PrA). **b** (Top) SEM images of COM crystals grown in the absence of inhibitor and the presence of CA or binary combinations of CA with polyphenols. (Bottom) Schematical illustrations of binding specificity with inhibitors. **c** Variations in COM [001]/[010] aspect ratio with increasing concentrations of binary inhibitors at displayed ratios. Error bars are two standard errors from more than 100 individual measurements. Lines are guides for the eye. **d** Inhibition percentage of COM crystal growth as a function of the concentration of single or binary inhibitors (upper horizontal axis: EA). Lines are guides for the eye and error bars are two standard deviations from an average of 3–5 measurements. **e** Cooperative index (CI) of CA/polyphenol binary inhibitors on COM crystal growth kinetics. Bovine serum albumin, BSA, chondroitin sulfate A, C_4S. CI = $(R)_1/(R_x)_1 + (R)_2/(R_x)_2$, $(R_x)_i$ is the concentration of a single inhibitor that inhibits crystal growth by x (inhibition percentage), and $(R)_i$ is the concentration of inhibitor i in binary inhibitor that has the identical inhibition percentage.

crystals harvested in CA/polyphenol pairs all display a smaller average aspect ratio than that in either inhibitor separately (Supplementary Fig. 2). Among the investigated inhibitor pairs, the CA/GaA and CA/PGA inhibitor pairs exhibit a more remarkable decrease in aspect ratio than others, implying strong synergistic cooperativity.

The growth rate of COM crystals was measured, using an ion-selective electrode (ISE) to track the temporal depletion of free Ca^{2+} ions in supersaturated CaOx solution[9,29], to assess quantitatively the inhibition performance of selected inhibitor pairs that was evaluated by inhibition percentage (%) defined as % = $(1\text{-}r_{inhibitor}/r_{control})$ *100. Figure 1d shows inhibition percentages of individual and binary inhibitors on COM growth which increase monotonically with increasing inhibitor concentration. In the selected concentration ranges of inhibitors (e.g., $C_{EA} < 1.5$ μM and $C_{other\ inhibitor} < 1$ mM), only EA displays complete growth cessation. Among selected natural polyphenols, the inhibition performances of EA and GaA outperform CA, far superior to PGA and PrA. The inhibition percentage of PrA is the lowest, suggesting the weakest growth suppression that may be

associated with its kink-blocking inhibitory action mode. However, the addition of either natural polyphenol to CA-containing solutions enforces greater inhibition performance than CA on its own, indicating synergetic activity. The stronger inhibition on COM growth imposed by two potent inhibitors, like CA/EA and CA/GaA pairs, is reasonably expected than that by either inhibitor. Interestingly, the combination of CA/PGA, which pairs a potent and a weak inhibitor, results in an enhanced growth suppression comparable to binary potent inhibitors. The pair of CA/PrA displays a slight enhancement of growth suppression at low CA concentrations but a negligible synergy at high concentrations.

A rigorously quantitative analysis of the cooperative effects of COM growth inhibitors was assessed by the combination index (CI), $CI = (R)_1/(R_x)_1 + (R)_2/(R_x)_2$[39,41]. Here, $(R_x)_i$ represents the concentration of constitute i used as an individual inhibitor that suppresses COM growth by x percent inhibition, and $(R)_i$ is the concentration of constitute i in a binary mixture to achieve the same percent inhibition. This mathematical expression facilitates the comparison of inhibitor pairs that display synergism ($CI < 1$), additivity ($CI = 1$), or antagonism ($CI > 1$). The weight-averaged CI values of each inhibitor pair are plotted in Fig. 1e, compared with two known inhibitor pairs of CA with urinary proteins, bovine serum albumin (BSA) or chondroitin sulfate A (C_4S)[39]. It was found that the combinations of CA with natural polyphenols all display much greater synergistic activity than those reported ones. Note that although EA alone leads to nearly complete growth cessation, the combined use of two potent inhibitors, that are EA and CA, is not necessarily the optimal formula to achieve the maximal growth suppression of COM crystals. The two most synergistic cooperativity cases are observed in CA/GaA and CA/PGA inhibitor pairs, which display only one-third CI value of the reported strongest inhibitor combination of CA-C_4S[39]. The result suggests the far superior inhibition efficacy of CA/GaA or CA/PGA inhibitor pair on COM crystallization, which may be used as drug candidates for the treatment of CaOx kidney stones.

Microscopic assessment of COM growth inhibition synergy. Microscopic evidence of synergistic cooperativity of CA/natural polyphenol inhibitor pairs was extracted from time-elapsed in situ atomic force microscopy (AFM) measurements that probe the molecular process of COM (100) surface growth[3,7]. Working with a supersaturated growth solution ($S = 2.4$) containing 150 mM NaCl at $pH = 6.4 \pm 0.4$ as a control group, we observe spiral growth from a screw dislocation which is consistent with previous reports in water medium[30]. The (100) surface exhibits tear-shaped hillocks bound by (001), (021), and $(12\bar{1})$ steps (Fig. 2a). The addition of GaA to the pure growth solution enforces the corrugated step edges with time and triggers the appearance of protrusions along the direction of step advancing (Fig. 2b). We further scrutinized inhibitor effects on the velocity of step propagation. Step velocity, v, in all growth directions, was measured from sequential images through continuous scanning, and the relative step velocity v/v_0 was reported, where v_0 is the step velocity of the control group in the absence of inhibitors. The correlation between v/v_0 and the concentration of the inhibitors demonstrates that binary inhibitor combinations impose stronger growth impedance than CA alone, leading to the dramatic decrease of step velocity in all growth directions in COM (100) surface (Fig. 2c–e). The addition of either a step pinner, GaA, a kink blocker, PrA, or EA or PGA to CA acting as a dual inhibitor of both step pinner and kink blocker substantially enhances growth suppression at all tested inhibitor concentrations relative to that with CA alone, implying strong synergy between these inhibitors. Surprisingly, the kink blocker, PrA, only decreases v along (001) step by up to 50% at 0.26 mM on its own (Supplementary Figs. 4i and 5) but exhibits 72% inhibition percentage at about 0.034 mM upon the addition to CA-containing solutions, signifying strong synergy between the combined CA (a dual inhibitor) and PrA (a kink blocker). The inhibitor pair CA/EA both exhibiting step pinning and kink-blocking inhibitory action elicits the nearly identical suppression of step propagation with CA/GaA inhibitor pair wherein GaA only functions as a step pinner along (100) and (021) steps. Either of these two inhibitor pairs exhibits a little weaker inhibition than CA/PrA pair at low CA concentrations ($C_{CA} < 0.023$ mM) but stronger retardation at high CA concentrations ($C_{CA} > 0.023$ mM).

The cooperativity of inhibitor pairs can be quantified by isobolograms (Fig. 2f–h, Supplementary Discussion 2 and Supplementary Figs. 9 and 10)[37,39], an analytical method commonly employed in the performance test of drug combinations, in which the doses of inhibitor pairs required to retard v by a certain percentage are compared with the sum of the responses to each inhibitor applied individually. When the two inhibitors displayed the additive effect, the pairing concentration values (solid symbols) will lie near or along the solid lines that are connected with the data of individual inhibitors (open symbols). The leftward shifts of concentration of binary inhibitor combinations from the solid lines signify a synergistic effect, whereas the rightward shifts of those from the line indicate an antagonistic effect[39]. It is evident that the paired concentrations of CA/EA, CA/PGA, CA/GaA, and CA/PrA are all located below the respective solid lines, corroborating the strong synergistic cooperativity of these inhibitor pairs.

Theoretical modeling of synergistic cooperativity between growth inhibitors. Synergistic cooperativity in suppressing v between a dual inhibitor (acting as both a step pinner and kink blocker) and another dual inhibitor, a step pinner, or a kink blocker could be understood within the realm of common crystal growth models. For example, a step pinner lowers step velocity by increasing the step curvature and depressing the crystallization driving force[33], which works in parallel with another step pinner that further reduces the crystallization driving force of curved steps by diminishing step curvature (Fig. 3a). It is also possible that a kink blocker lowers the kinetic constants of growth by blocking available kink sites, which works cooperatively with the depression of crystallization driving force through step curvature enforced by step pinners[33]. According to these inhibitory action mechanisms, the analytical models for describing synergy between inhibitor pairs were developed to understand the correlation between the bulk concentration of individual inhibitors and the velocity of step propagation (see details in Supplementary Discussion 3 and Supplementary Fig. 11). It is noted that these models are established on the basis of two common growth inhibition mechanisms (i.e., step pinning and kink blocking) and experimental measurements, as well as the extensions of cooperative models reported by Weaver et al. [33] and Vekilov et al. [37,42]. But herein we considered much more complicated combinations of two inhibitors wherein each inhibitor can function as a dual inhibitory action of both step pinning and kink blocking. Figure 3b–e depicts the theoretical prediction of synergy between inhibitors in comparison with experimental data.

The theoretical v/v_0 values in CA/PGA inhibitor pair reproduce relatively well experimental data in the tested concentrations, demonstrating the synergistic effect of two dual inhibitors on step propagation (Fig. 3b). The consistency between the results of the model prediction and the experimental values was also observed in CA/EA or CA/GaA combination (Fig. 3c, d), signifying the inhibitory synergy between a dual inhibitor and a step pinner as

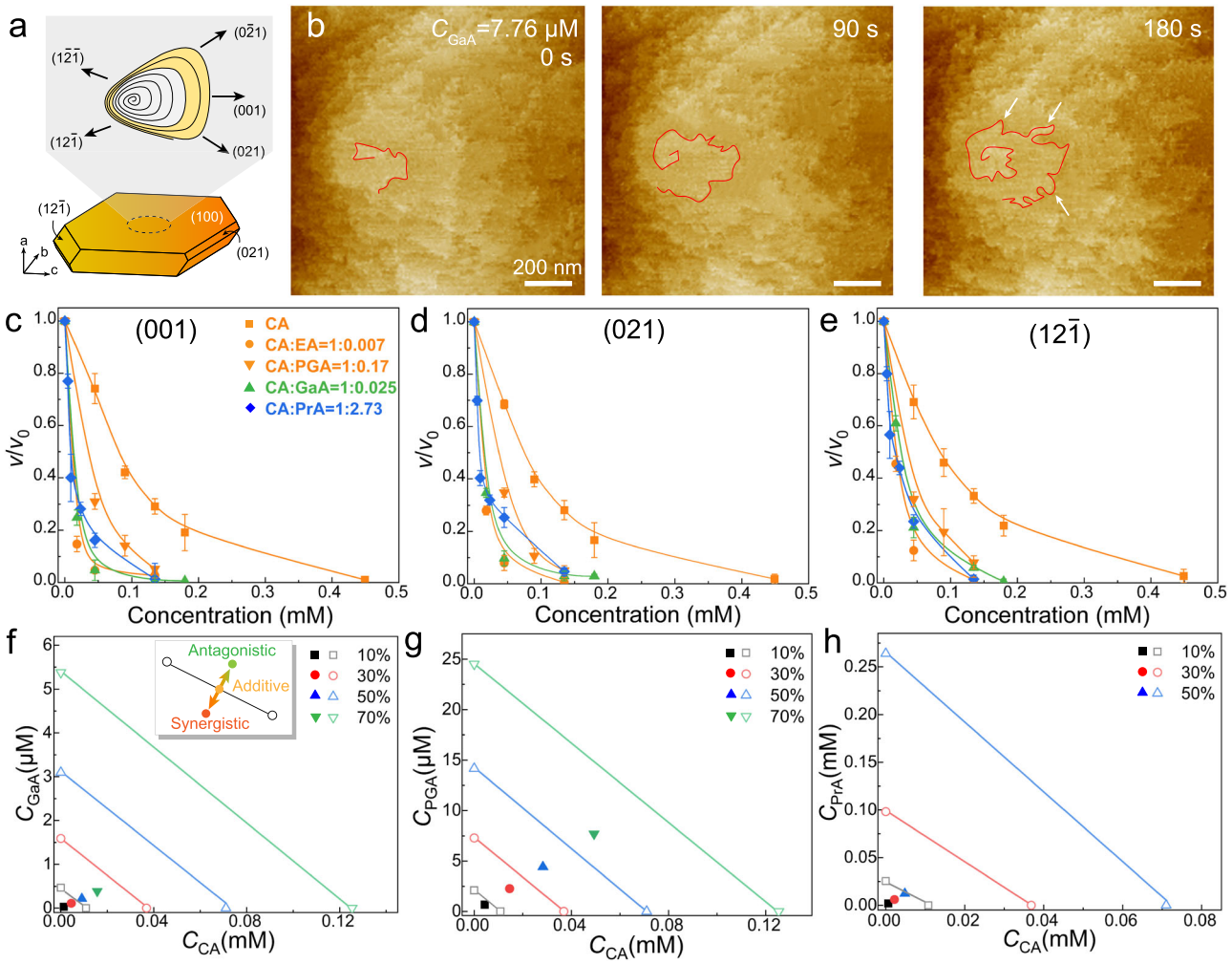

Fig. 2 Synergy of inhibitor pairs on retarding step propagation. a Schematic of a spiral hillock on COM (100) surface. **b** Time-elapsed in situ AFM images showing spiral propagation of steps on (100) surface at a supersaturation of 2.4 with 7.8 μM GaA. Red curved lines outline the step edge of the spiral hillock, and white arrows mark the protrusions that are formed at step edges. **c**–**e** Decrease of step velocity, v, of layer advancement relative to that in the absence of inhibitors, v_0, along (001) step plane (**c**), (021) step plane (**d**), and (12$\bar{1}$) step plane (**e**) with increasing concentrations of CA in inhibitor pairs at the displayed ratios. Error bars represent the standard deviation from an average of 15–25 measurements of v. Lines are guides for the eye. **f**–**h**, Isobolograms depicting the synergistic retardation of v by inhibitor pairs of GaA/CA (**f**), PGA/CA (**g**), and PrA/CA (**h**). Open symbols represent the concentrations of individual inhibitors that elicit a certain percentage of inhibition. Solid lines correspond to additive cooperativity between the paired inhibitors for a certain percentage of inhibition (10–70%). Solid symbols indicate the concentrations of the paired inhibitors that evoke the same inhibition. Leftward shifts of symbols from the respective solid lines suggest synergistic cooperativity.

well. Besides, the predicted values of step velocity v/v_0 in CA/PrA inhibitor pair capture general trends of experimental data. Nevertheless, deviations were evident at high concentrations of CA/EA, CA/GaA, and CA/PrA (Fig. 3e), which may be accredited to other effects different to step pinning or kink blocking such as surface solvation[43,44] and local strains[9,45].

We further derive the correlation between the velocity of a step, v/v_0, and the concentrations of CA and natural polyphenols (PGA, EA, GaA, or PrA) (see Supplementary Equations 18–20) to predict the cooperativity of binary inhibitors at other ratios. Note that the governing parameters of these models were derived independently by fitting the measured step velocities in the presence of each inhibitor and summarized in Supplementary Tables 1–3. Three-dimensional surfaces [$v/v_0 = f\,(C_{CA}, C_{polyphenol})$] are generated in Fig. 3f–i and Supplementary Fig. 12. The lines on coordinate planes represent the theoretical change of step velocity, $v/v_0(0, C_{polyphenol})$ or $v/v_0(C_{CA}, 0)$, as a function of the concentration of an inhibitor alone. All the concentrations of binary pairs on an intersection line of the 3D surface with a plane perpendicular to the v/v_0-axis exhibit identical values of v/v_0 and thus the same inhibition percentage. A concave-shaped intersection line, which is similar to leftward shifts of concentration pairs from the solid lines in Fig. 2f–h, indicates the synergistic cooperativity[39]. Note that these figures may resemble those reported in ref. [37] (extended data Fig. 5), given the similar behaviors of cooperative inhibition by binary inhibitors. But they are derived on the basis of different sources of experimental data and applicable to different substance systems. Interestingly, we observed the synergy in all four inhibitor pairs on the (100) surface. These results provide insights for developing an effective therapeutical strategy through binary inhibitor drug combinations to prevent and treat CaOx kidney stones.

Enhanced reduction of COM crystal cytotoxicity and adhesion to human proximal tubular (HK-2) cells using inhibitor combinations. The formation of kidney stones may be prevented by diminishing CaOx crystallization, crystal-cell interactions, and cell injury through molecular design[5,16]. Some COM growth

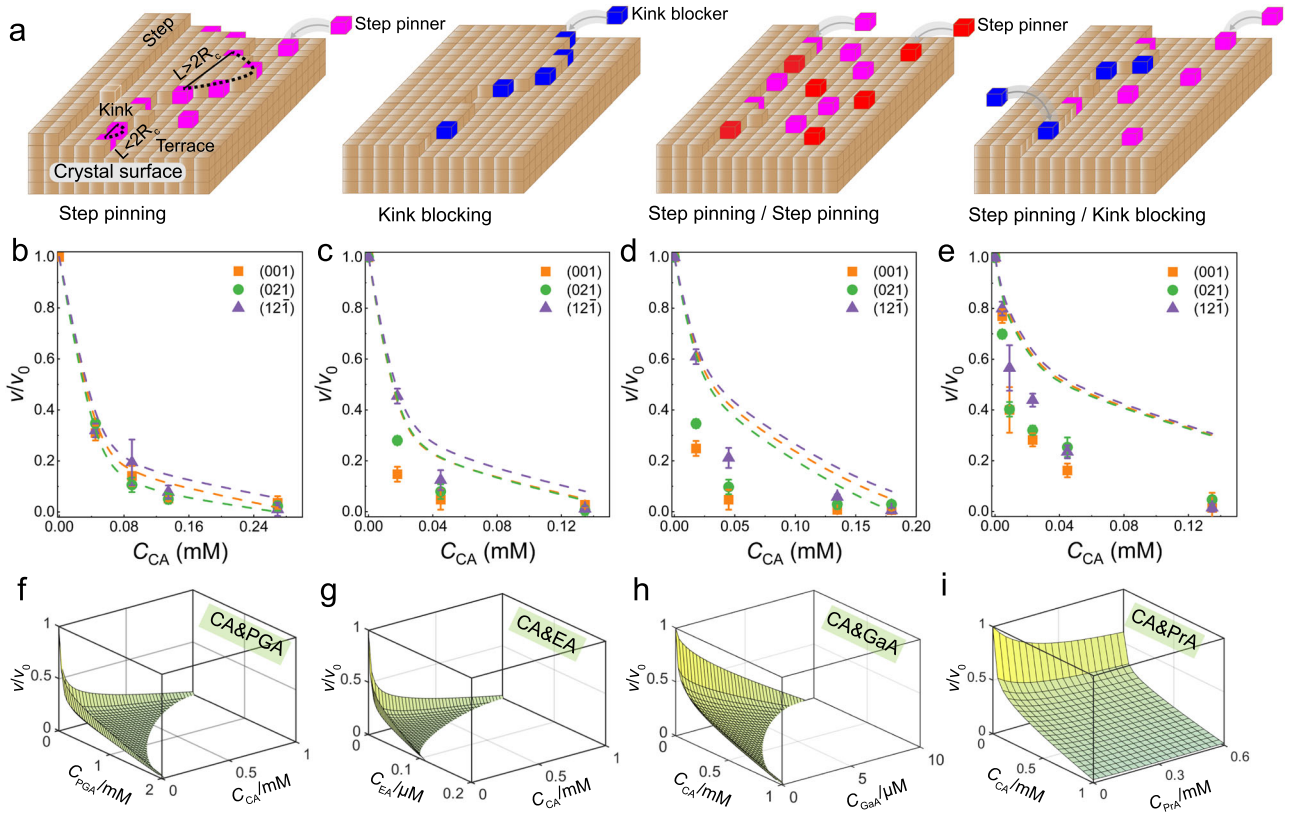

Fig. 3 Theoretical modeling of the inhibitory action of pairs between a step pinner and a step pinner, or a kink blocker on step advancement. **a** Schematic illustration of single or binary inhibitors suppressing step spreading *via* step pinning or/and kink blocking. **b**–**e** Dependence of step velocity v relative to that in the absence of any inhibitor v_0 (v/v_0) on CA concentrations in CA/PGA 1:0.17 (**b**), CA/EA 1:0.007 (**c**), CA/GaA 1:0.025 (**d**), and CA/PrA 1:2.73 (**e**), Solid symbols are the experiment values, and dashed lines are the fits to Eqs. (S22–24). Error bars are the standard deviation from an average of 15–25 measurements of v. **f**–**i** The correlation between the theoretical step velocity v relative to that in pure solution v_0 and the concentrations of CA and polyphenols (PGA, EA, GaA, PrA) along (001) step plane. Derived values of ξ, K_{LB}, and K_{LP} of a single inhibitor are listed in Supplementary Tables 1–3. The surface area per adsorption site $S_0 = 0.12\,nm^2$ was estimated from the structure of COM crystals.

inhibitors can suppress the adhesion of crystals to cells such as citrate, polyphosphates, Tamm−Horsfall protein, and chondroitin sulfate[16,46–48]. The surface of human proximal tubular (HK-2) cells is rich in anionic sites like anionic phospholipids, sulfate esters, sialic acid, uronic acid, and hyaluronan[21], which can be bonded to Ca^{2+} exposed on COM crystal surfaces. These ionic interactions lead to the adhesion of crystals to cells (Fig. 4a) and can be weakened by inhibitors[21]. It was reported that the three carboxyl groups of CA molecule can be bonded on COM crystal (100) surface via electrostatic and H-bond interactions[7], decreasing Ca^{2+} exposed density on the surface of crystals and suppressing crystal adhesion to the cell surface (Fig. 4a). Here we found that four natural polyphenol molecules (GaA, EA, PGA, and PrA) can bind to (100) surface by H-bonds and electrostatic interactions (Supplementary Fig. 7) and revealed the synergistic adsorption of studied inhibitor combinations on COM (100) surface. Further, we investigated the synergistic cooperativity of CA with each polyphenol combination on the effects of cell injury and crystal adhesion.

Adhesion of crystals to the cell surface can directly induce crystal cytotoxicity by phagocytosing into intracellular phagosomes that fuse with lysosomes or indirectly trigger cell necrosis through an auto-amplification loop involving the release of damage-associated molecular patterns[49]. To explore the cooperativity of inhibitor pairs on crystal cytotoxicity, we chose an in vitro model with direct exposure to COM crystals for the detection of short-term cell injury. Confluent human proximal tubular cells (HK-2) were exposed for the indicated times to COM crystals in the presence and absence of a single inhibitor or binary inhibitors. By assessing the intracellular esterase activity, it was found that after being exposed to COM crystals for 24 h, HK-2 cells displayed decreased integrity of cell membrane and reduced cell viability compared with the control that was only exposed to DMEM/F12 medium (Fig. 4b)[50]. The addition of CA inhibitor decreased the number of dead cells by about 50% (Fig. 4c). When the inhibitor combinations were employed, we observed the synergistic cooperativity in decreasing crystal cytotoxicity. The efficacy of increasing cell viability between CA/PGA and CA/PrA pairs was comparable but weaker than that of CA/GaA and stronger than CA/EA.

Lactate dehydrogenase (LDH) is a type of cytoplasmic enzyme released to extra cells when the cell membrane ruptures[51]. Then the amount of LDH released was considered a sign of cell membrane integrity (Fig. 4d). LDH release increased to almost 277.14% (±36.02%) after COM crystals exposure compared to the control but decreased to195.17% (±2.46%) with 200 μM CA. Lower LDH release in the presence of inhibitor pairs suggests the synergy of CA and each polyphenol combination in maintaining cell membrane integrity. The values in Fig. 4d also demonstrate that CA/GaA (110.87% ± 8.67%) and CA/PrA (115.73% ± 3.32%) outperform other inhibitor combinations to maintain cell viability.

Crystal adhesion is not only the prerequisite for cell necrosis but also crucial for triggering crystal aggregation[14,49]. Therefore, the cooperative anti-adhesive effects of inhibitor pairs on COM crystals to HK-2 cells were also investigated in vitro by quantifying the number of adhered crystals (Fig. 4e). It was found that CA shows 30% COM adhesion inhibition compared to the control wherein the inhibitor is absent. The treatments of

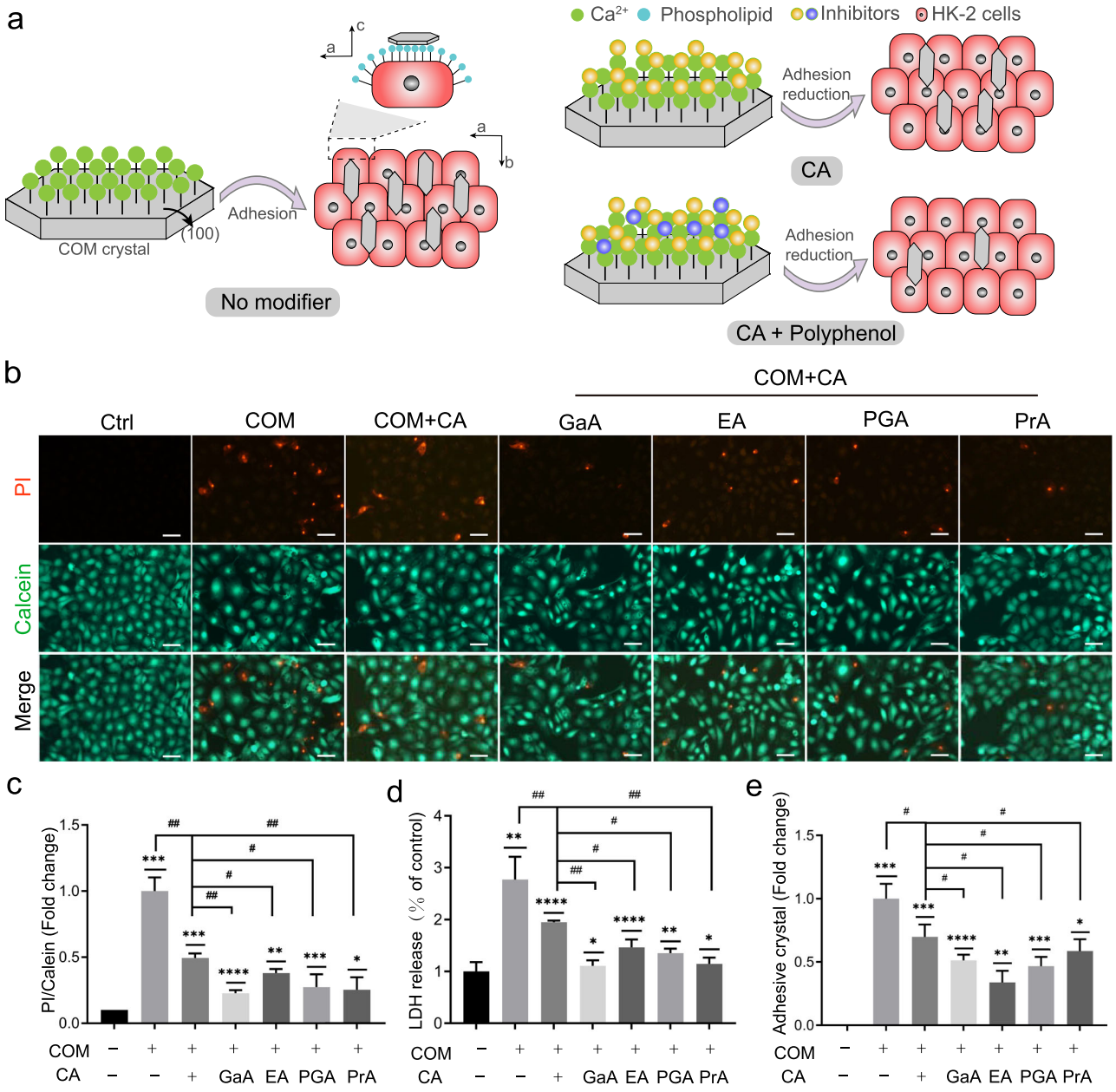

Fig. 4 Cooperative reduction of inhibitor pairs on crystal cytotoxicity and adhesion to human proximal tubular (HK-2) cells. a Schematic of the adhesion between COM crystals and HK-2 cells in the absence and presence of inhibitors. The less Ca^{2+} density exposed on (100) surface, the less the number of crystals adhered to the HK-2 cells. **b** Representative images of calcein (live, green)-propidium iodide (PI, dead, red) staining ($n = 6$ from three donors). Scale bar, 50 μm. Cultured HK-2 cells were treated with 100 μg mL^{-1} COM, with or without 200 μM CA, and binary combinations of 200 μM CA with 20 μM GaA, 20 μM EA, 40 μM PGA, or 200 μM PrA for 24 h. **c**–**e**, Statistical analyses on the ratio of PI/calcein positive cells (**c**), total protein-corrected LDH release ($n = 20$ from five donors) (**d**), and adhered COM crystal number (**e**). Data are present as mean ± SEM. Compared with the control group, $^{*}p < 0.05$, $^{**}p < 0.01$. Compared with CA-treated groups, $\#p < 0.05$, $\#\#p < 0.01$.

inhibitor pairs led to approximately 50% reduction of adhered crystals, remarkably greater than that with CA alone. The efficacy of crystal adhesion inhibition between CA and EA pair was superior to that of CA/GaA, CA/PGA, and CA/PrA pairs. Note that the greater performance of CA/EA pair on reduction of adhesive COM crystals than CA/GaA may be due to stronger adsorption of EA on COM crystal surface (Supplementary Fig. 7).

Inhibitor pairs synergistically reduce renal CaOx deposition and kidney injury in vivo. The promising in vitro results of inhibitor combinations on suppressions of CaOx crystallization and cell adhesion motivated us to perform an in-vivo proof-of-concept study in a mouse model of CaOx-induce nephrocalcinosis. Following a previously reported protocol, CaOx kidney stones in mice were induced by injecting glyoxylate (Gly), which promotes the formation of hyperoxaluria[52]. Concurrently, mice were treated with CA/polyphenol pairs subcutaneously once daily at indicated doses for 6 days before sacrifice. Renal CaOx crystals (Fig. 5a) and kidney sections stained by Von-Kossa staining (Fig. 5b and Supplementary Fig. 15) reveal a reduction in renal CaOx deposition with CA and inhibitor combinations, which is significant for all treatment groups compared to the Gly-treated group. The quantification results presented in Fig. 5d show a

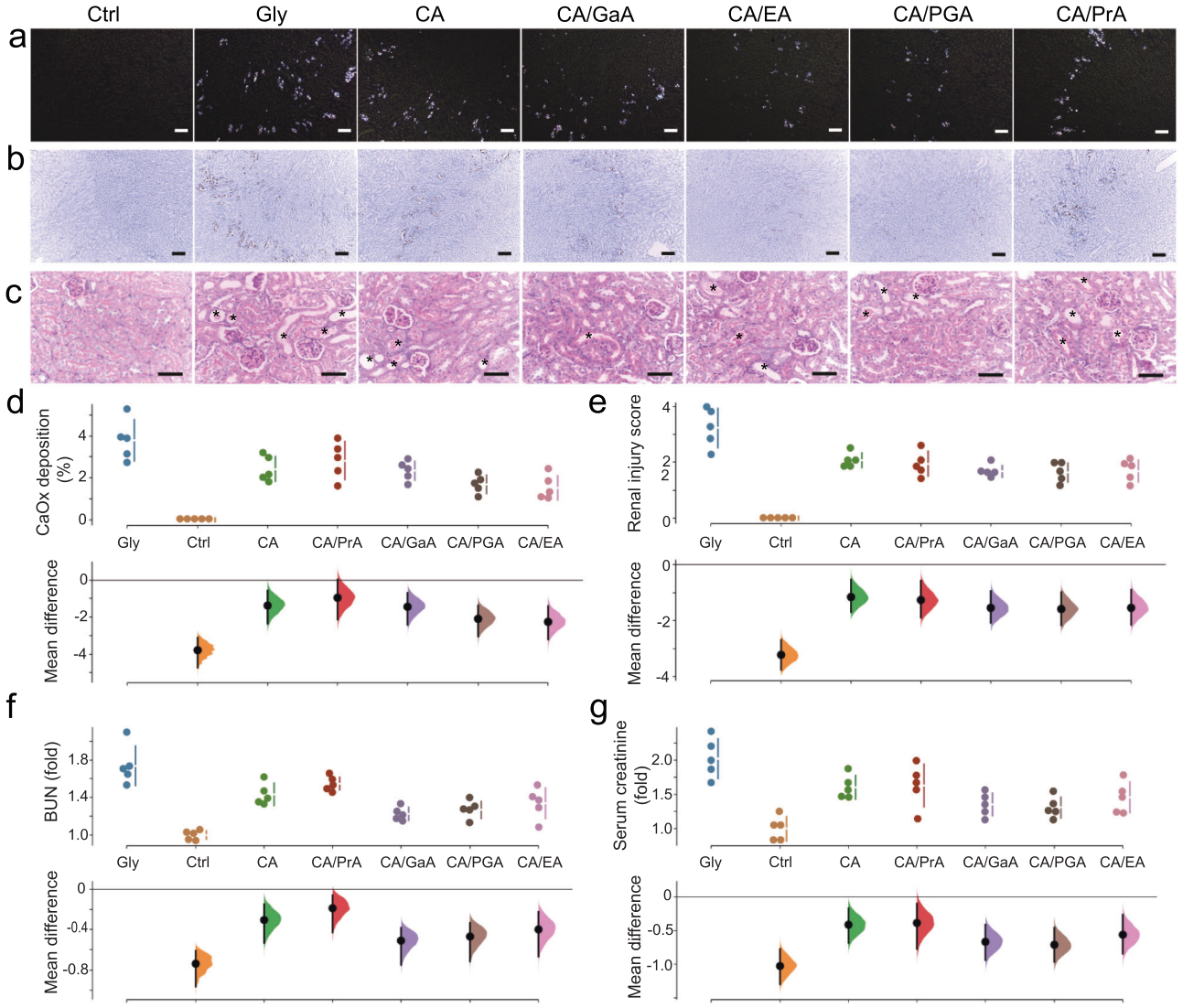

Fig. 5 Inhibitor combinations reduce renal CaOx deposition and injury in a mouse model of renal CaOx crystallization. C57BL/5 mice received an intraperitoneal injection of glyoxylate to induce renal CaOx crystallization and were concurrently treated with indicated concentrations of CA and CA/polyphenol pairs for 6 constitutive days. **a** Morphologic distribution of renal CaOx crystals using polarized-light optical microphotography (scale bar: 50 μm). **b** Representative images of Von-Kossa staining of kidney sections (scale bar: 50 μm). **c** Representative images of stained kidney sections with periodic acid–Schiff stain and highlighted areas of tubular injury (scale bar: 50 μm). **d, e** Quantified CaOx crystal deposition (**d**) and scored kidney injury (**e**) in kidney sections. **f**, **g** Plasma blood urea nitrogen (BUN, **f**), and serum creatinine concentration (**g**) were measured on day 7. The raw data was plotted on the upper axes with line breaks denoting the mean value of each group and lines indicating the standard deviation. The mean differences for six comparisons against the shared positive control, Gly, were plotted as bootstrap distributions on the bottom axes. Each mean difference is depicted as a dot and each 95% CI is indicated by the ends of the vertical error bars.

relatively strong synergy of CA/PGA pair on reduction of renal crystal deposition, in line with the in vitro result (Fig. 1e). Surprisingly, the combination of CA and EA exhibits a superior in vivo inhibition efficacy in the reduction of crystal deposition than other remaining pairs. Additionally, the synergistic performance difference of CA/GaA binary combination between in vitro and in vivo assays may be associated with the metabolism of GaA, which leads to only about 36.4% of the ingested GaA dose presented in urine[53]. CA/PrA inhibitor pair displayed little synergistic effect in vitro studies, whereas it exhibits a slight antagonism in reducing CaOx crystal formation in renal. Overall, the synergy of binary inhibitor combinations has been successfully demonstrated in both in vitro and in vivo studies (Figs. 1e and 5d), which implies the in vivo validation of the proposed strategy using binary inhibitor combinations as a potential prevention and/or treatment method of kidney stones.

The metabolism of Gly in mice leads to the formation of hyperoxaluria, which promotes renal CaOx crystallization and causes kidney injury, forming renal calculus stones[52]. Damaged renal tubular epithelial cells are conducive to crystal deposition while attached crystals further deteriorate cell damage[13,54,55]. The kidney injury can be reduced by the administration of CA inhibitor, especially binary inhibitor combinations, as evidenced by periodic acid–Schiff staining of kidney sections and scoring of tubular injury (Fig. 5c, e). Consistent with the in vitro synergistic performance, CA/GaA and CA/PGA combinations display superior efficacy of kidney injury reduction to CA alone, CA/EA, or CA/PrA pair. Notably, the in vivo synergy of CA/EA pair to reduce kidney injury is also evident in comparison with CA alone. Moreover, the measurements of plasma blood urea nitrogen (BUN) and serum creatinine reveal the improved excretory kidney function after treatments with CA alone or

CA/polyphenol pairs compared to the Gly-treated group (Fig. 5f, g). Again, the binary inhibitor pairs of CA/GaA, CA/PGA, and CA/EA all display synergy performance than CA alone. The enhanced improvement of kidney function in the presence of binary inhibitor pairs seems to agree with their efficacy in the reduction of kidney injury. The less effective inhibition performance of CA/PrA combination in reducing crystal deposition and renal damage may be related to the poor absorption of PrA on its own[56]. Together, these results support in vivo efficacy of CA/polyphenol combinations to synergistically reduce renal CaOx crystallization and deposition in the kidneys. The study further confirms the kidney-protective effects of inhibitor combinations involved, presumably due to reduced CaOx crystallization and tissue interactions mediated by inhibitor pairs. Moreover, when inhibitor combinations of CA and polyphenols were developed as potential therapeutics for preventing human kidney stones, an oral formulation could be possible due to the renal excretion of the studied polyphenols[53,56–58]

Discussions

Citrate is one of the urinary constituents, and its inhibition on CaOx crystallization and crystal-cell interactions in renal urine has been well recognized[59], by which the only commercial drug alkali citrate was developed for preventing the recurrence of CaOx stones since 1980s[55]. However, the use of alkali citrate leads to a series of adverse events such as hyperkalemia and gastrointestinal side effects[59,60], and thereby the development of new inhibitor drugs or their combination is desired. The conventional use of a single inhibitor often requires a high level of drug concentration to completely suppress CaOx crystalization which, nonetheless, results in increased toxicity and unfriendly administration compliance. To address such a problem, the combined use of binary inhibitors to boost inhibition performance with the minute amount of concentration could be an alternatively promising approach. Nowadays, drug combination has been widely recommended in the development of drug formulations, which offer superior therapeutic outcomes based on the cooperativity of different targets aimed by different drugs. On the contrary, the cooperativity between crystal growth inhibitors is realized by targeting the same CaOx COM crystal.

Few rare studies explored the combined use of inhibitor pairs on CaOx crystallization. Rimer et al. [39] found the synergistic effects between urinary proteins (BSA, C4S, Tf) and CA on CaOx crystallization, yet the applications of inhibition synergy on COM crystal-cell interaction were not examined. Here, we reported the unparalleled synergism of binary inhibitor pairs between CA and natural polyphenols (GaA, EA, PGA, or PrA) on the growth suppression of pathological COM crystals. The inhibition performance of CA/GaA combination on suppressing CaOx crystallization is 3-fold greater than that of a reported combination of CA/C_4S and four-fold higher than that of CA alone. Further, the synergistic cooperativity in suppressing crystal growth was observed not only between a dual inhibitor (functioning as both a step pinner and a kink blocker) and another dual inhibitor or a step pinner but also between a dual inhibitor and a kink blocker. Unexpectedly, we found that the synergistic efficacy of inhibitor pairs between a dual inhibitor and a kink blocker could be even stronger than that between a dual inhibitor and a step pinner. The antagonistic cooperativity between a step pinner and a kink blocker was reported on retarding crystal growth, originating from the reduction of step line tension, a thermodynamic prerequisite for the adsorption of molecules of a kink blocker at steps[37]. But stronger antagonism between a step pinner and a kink blocker is projected for their joint action on the rate of two-dimensional nucleation of new crystal layers, rather than step velocity (v), the rate of step propagation[37]. We posit that the synergism between these three types of inhibitors (i.e. step pinner and kink blocker, step pinner, and kink blocker) results from the reduction of growth kinetic constants paralleled with the depression of crystallization driving force, as illustrated in Fig. 3. The discovery of the strong synergy between inhibitors, i.e. synergistic cooperativity, could be potentially utilized for boosting inhibition performance of pathological CaOx crystallization. The idea was successfully demonstrated through an in-vivo proof-of-concept study in a mouse model of CaOx-induce nephrocalcinosis wherein the combinations of CA/PGA, CA/EA, and CA/GaA show synergistic reductions of renal CaOx crystal deposition and kidney injury.

In summary, our findings revealed that the combinations of CA and natural polyphenols display superior inhibition efficacy on crystal growth and crystal-cell interactions to that of inhibitor alone, suggesting an innovative therapeutic modality for CaOx-related kidney stones through the formulation of binary inhibitor combinations. The synergistic cooperativity on suppression of CaOx crystallization was resulted from the reduction of growth kinetic constants and/or the depression of crystallization driving force and was found not only between a dual inhibitor and another dual inhibitor or a step pinner but also between a dual inhibitor and a kink blocker. Further, we found the synergy of inhibitor combinations on the reduction of COM crystal cytotoxicity and adhesion with human proximal tubular (HK-2) cells. The persistence of synergistic cooperativity of inhibitor pairs was also demonstrated by the in-vivo mice model study, showing boosting inhibition efficacy on CaOx stone formation. Together, we describe the development of an effective class of COM inhibitor pairs that act on the suppression of two common formation stages of CaOx stones, namely crystallization and crystal adhesion to the cells. In a broader context, our results highlight inhibitor-crystal interface interactions mediated by the crystallization dynamics and structures as a significant modifier of the shapes and patterns of crystalline structures in nature and industry that may potentially impact diverse areas spanning materials design and synthesis to pharmaceuticals.

Methods

Materials. The following reagents were purchased from Aladdin: ellagic acid (EA, ≥96%), gallic acid (GaA ≥99%), pyrogallic acid (PGA, ≥99%), $CaCl_2$:$2H_2O$ (> 99%), and NaCl (≥99.5%). Protocatechuic acid (PrA, ≥98%), $Na_2C_2O_4$ (≥99.0%), and citrate (CA, >99.5%) were purchased from Sigma-Aldrich. All reagents were used as received. Deionized water (18.2 MΩ) was used throughout the experiments.

Bulk crystallization assays. The inhibition performance of four inhibitor pairs (CA/EA, CA/PGA, CA/GaA, and CA/PrA) was evaluated by bulk crystallization. The crystallization was performed in a 50-mL glass beaker with 25 mL solution containing 0.56 mM $CaCl_2$: 0.56 mM $Na_2C_2O_4$: 150 mM NaCl: x inhibitor. The beaker was then placed on a hot plate (37 °C) for 3 days under quiescent conditions. A coverslip (20 × 20 mm) was placed at the bottom of a beaker to collect crystals. The ratios of CA/EA, CA/PGA, CA/GaA, and CA/PrA between the two inhibitors are 1:0.007, 1:0.17, 1:0.025, and 1:2.73, respectively. The concentrate range of x relative to CA is 0–0.18 mM. The coverslips with collected crystals were gently removed from the beaker, washed with water and 95%(v/v) ethanol, and dried at room temperature for SEM characterization.

The influence of these inhibitor combinations on the growth kinetics of COM crystals was assessed by Ca^{2+} ions selective

electrode (ISE, Thermo Scientific, Orion 9720BNWP). The depletion of free Ca^{2+} concentration in the growth solution was recorded over the course of crystal growth at a stirring rate of 400 rpm. About 5 mg COM crystal seeds were added into a 100 mL growth solution. The growth solution contains 0.31 mM $CaCl_2$: 0.31 mM $Na_2C_2O_4$: 150 mM NaCl: x inhibitor where x is 0–0.45 mM (relative to CA) and the ratios of inhibitor pairs are the same as aforementioned. Each experiment was replicated at least twice. The growth of COM crystals results in the depletion of free Ca^{2+} in solution, the slope of which in the presence of inhibitors was compared with that in the absence of inhibitors to derive the inhibition percentage.

Preparation of crystal seeds. Seeds of COM crystal used for AFM measurements were prepared by spontaneous crystallization on coverslips which are laid down in a supersaturated CaOx solution. COM crystals exposed (100) basal surface were prepared from a supersaturated solution containing 0.56 mM $CaCl_2$: 0.56 mM $Na_2C_2O_4$:150 mM NaCl, whereas COM crystals mostly exposed (010) surface were prepared from a supersaturated solution containing 0.56 mM $CaCl_2$: 0.56 mM $Na_2C_2O_4$: 150 mM NaCl: 2.02 mM $NaHCO_3$. The crystals were produced under quiescent conditions for 3 days at 37 °C. Then the coverslips with crystals were taken and slightly washed with deionized water for AFM experiments.

In situ atomic force microscope (AFM). The dynamics of surface growth of COM crystals were captured by time-resolved in situ AFM images on a Dimension Icon (NanoScope V, Bruker). The glass slip with a thin layer of thermally curable epoxy was placed in an oven for about 40 min at 50 °C to partial cure of epoxy layer. Then a coverslip with COM crystals was gently pressed on this glass slip with partially cured epoxy to transfer crystals. The sample was then placed in an oven at 50 °C for another 1 h to completely cure the epoxy. AFM images were collected in Peakforce tapping mode using Scanasyst fluid+ probes (silicon nitride with reflective Au, 0.7 N/m spring constant) in the fluid. Image sizes ranging from 1 to 5 μm were collected using a scan rate of 3 Hz at 256 lines per scan. Growth solutions at pH 6.4 ± 0.2 with a composition of 0.31 mM $CaCl_2$:0.31 mM $Na_2C_2O_4$:150 mM NaCl: x mM inhibitors (where $x = 0$–0.45 relative to CA) were freshly prepared within 1 h of each measurement. The ratios of CA/natural polyphenol inhibitor pairs are identical to the experiments used for bulk crystallization and ISE. The area of coverslips and AFM tips were kept hydrated with a 250 μL droplet of growth solution. The growth solution was refreshed every 10 min to maintain the constant solution supersaturation (see Supplementary Fig. 3). We measured the velocity of step advancement and changes in hillock morphology on COM (010) surface in the absence or presence of inhibitors. The reported step velocity (Fig. 2c–e) is the average of at least 15 measurements of different steps.

Cell experiments. Human proximal tubular cell line HK-2 was purchased from the ATCC (Manassas, VA) and cultured in DMEM/F12 medium containing 10% FBS and 1% penicillin and streptomycin (Gibco, Gaithersburg, MD) at 37 °C/5% CO_2. Cell viability was assessed using the Calcein/PI cell viability/cytotoxicity assay kit (Shanghai, Beyotime). After being seeded in 24-well plates for 48 h (upon reaching 100% confluency), HK-2 cells were treated with 100 μg/mL COM crystals (Supplementary Fig. 13) in DMEM/F12 medium premixed with CA or inhibitor pairs. 200 μM CA, 200 μM CA/20 μM EA, 200 μM CA/20 μM GaA, 200 μM CA/40 μM PGA, 200 μM CA/200 μM PrA were used. The relative cell viability with different inhibitors is shown in Supplementary Fig. 14. After a 24 h incubation, cell viability was measured by staining with Calcein/PI assay kit (Shanghai, Beyotime). Images (Calcein, 494 nm, green; PI, 535 nm, red) were recorded on a fluorescence microscope (Zeiss, Vert. A1). The number of red and green fluorescence dots was quantified. The identical cell viability experiment was also performed in 12-well plates to detect the LDH release, and the absorbance was analyzed at 490 nm according to the LDH kit instruction (Nanjing Jiancheng Bioengineering Institute). The adhesion property of CaOx crystals to HK-2 cells was quantified by culturing HK-2 cells with designed inhibitor pairs in DMEM/F12 medium for 30 min at 37 °C and 5% CO_2. Cells were then washed thrice with PBS, and images were collected on an inverted microscope with a bright field. The number of adhered crystals was quantified in at least 10 randomized fields per well.

Animal studies. A total of 35 male 8-week-old C57BL/6 mice, weighing approximately 18–22 g, were purchased from the Beijing Charles River (Beijing, China). After 1 week of acclimation, the mice were randomly divided into seven groups ($n = 5$): vehicle control group (Ctrl), mice received an intraperitoneal injection of normal saline; crystal control group (GLY), mice received an intraperitoneal injection of glyoxylate (75 mg per kg per body weight per day) for 6 constitutive days; treatment group 1 (GLY + CA), mice received an intraperitoneal injection of glyoxylate (75 mg per kg per body weight per day) and CA (50 mg per kg per body weight per day, a medium concentration that could achieve 50% reduction of tubular injury[61]) for 6 constitutive days, treatment group 2–5 (GLY + CA + GaA/EA/PGA/PrA), mice received an intraperitoneal injection of glyoxylate (75 mg per kg per body weight per day) and drug combinations: CA + GaA / EA / PGA/ PrA (total 50 mg per kg per body weight per day, wherein GaA:CA = 0.8:10, EA:CA = 1.4:10, PGA:CA = 1.2:10, PrA:CA = 7.3:10) for 6 constitutive days. The concentrations of inhibitors used are within the range of concentration at which the relative cell viability exceeds 99%. All mice were euthanized and samples of serum and kidney tissues were collected for further analysis on the 7th day of the experiment. All mice were housed under controlled temperature, humidity, and lighting. Experiments were conducted following the principles of the Institutional Animal Use and Care Committee of Nankai University.

Assessments of kidney injury and crystal deposition. Urea and creatinine assay kits (Nanjing Jiancheng Bioengineering Institute) were employed to measure serum creatinine concentration and blood urea nitrogen (BUN) concentration, following the manufacturer's instructions. Renal damage was assessed by kidney specimens stained by periodic acid Schiff (PAS) (Solarbio life sciences). Tubular dilation, protein cast, and brush border damage were quantitated by 10 images selected in random fields (200 magnification, AX10, Zeiss). The tubular injury index was evaluated by the percentage of areas of proximal tubular dilation, protein cast, or brush border damage per whole section and the score index was set from 0 to 10 (0–1, none; 1–2, <11%; 2–4, 11–25%; 4–6, 26–45%; 6–8, 46–75%; 8–10, >75%). The score for acute tubular necrosis was determined by adding the scores of each individual item. Kidney CaOx deposition was visualized using Von-Kossa staining kits (Solarbio), following the manufacturer's instructions. The area of CaOx crystal was quantified from ten or more randomly selected fields using Image J software.

Statistical analysis. Statistical results and graphs are presented as the mean ± standard deviation (SD.) and analyzed using GraphPad Prism (Version 8.0) unless otherwise stated. Ordinary one-

way ANOVA testing and two-tailed Student's testing were used for the comparison of a treatment to the negative control group and positive control group, respectively. For animal experiments, estimation graphics were plotted using the DABEST Python package in Python 3.6. The normality of animal data was assessed by D'Agostino and Pearson testing and found to be normally distributed. Statistical details of experiments are described in the figure legends.

Data availability

Additional experimental methods and data are available in the Supplementary Information of this paper. All data for the figures and other Supplementary Information that support this work are available upon reasonable request to the corresponding author.

Received: 23 December 2022; Accepted: 21 August 2023;
Published online: 02 September 2023

References

1. Dalbeth, N., Gosling, A. L., Gaffo, A. & Abhishek, A. Gout. *Lancet* **397**, 1843–1855 (2021).
2. Schantl, A. E. et al. Inhibition of vascular calcification by inositol phosphates derivatized with ethylene glycol oligomers. *Nat. Commun.* **11**, 1–17 (2020).
3. Poloni, L. N. & Ward, M. D. The materials science of pathological crystals. *Chem. Mater.* **26**, 477–495 (2014).
4. Orimo, H. The mechanism of mineralization and the role of alkaline phosphatase in health and disease. *J. Nippon. Med. Sch.* **77**, 4–12 (2010).
5. Wesson, J. A. & Ward, M. D. Pathological biomineralization of kidney stones. *Elements* **3**, 415–421 (2007).
6. Franceschi, V. R. & Nakata, P. A. Calcium oxalate in plants: formation and function. *Annu. Rev. Plant Biol.* **56**, 41–71 (2005).
7. Qiu, S. R. & Orme, C. A. Dynamics of biomineral formation at the near-molecular level. *Chem. Rev.* **108**, 4784–4822 (2008).
8. Moe, O. W. Kidney stones: pathophysiology and medical management. *Lancet* **367**, 333–344 (2006).
9. Chung, J. et al. Molecular modifiers reveal a mechanism of pathological crystal growth inhibition. *Nature* **536**, 446–450 (2016).
10. Kittanamongkolchai, W. et al. Risk of hypertension among first-time symptomatic kidney stone formers. *Clin. J. Am. Soc. Nephrol.* **12**, 476–482 (2017).
11. Gillen, D. L., Worcester, E. M. & Coe, F. L. Decreased renal function among adults with a history of nephrolithiasis: a study of NHANES III. *Kidney Int.* **67**, 685–690 (2005).
12. Gambaro, G. et al. The risk of chronic kidney disease associated with urolithiasis and its urological treatments: a review. *J. Urol.* **198**, 268–273 (2017).
13. Tsujihata, M. Mechanism of calcium oxalate renal stone formation and renal tubular cell injury. *Int. J. Urol.* **15**, 115–120 (2008).
14. Rodgers, A. L. Physicochemical mechanisms of stone formation. *Urolithiasis* **45**, 27–32 (2017).
15. Evan, A., Lingeman, J., Coe, F. L. & Worcester, E. Randall's plaque: pathogenesis and role in calcium oxalate nephrolithiasis. *Kidney Int.* **69**, 1313–1318 (2006).
16. Kletzmayr, A. et al. Inhibitors of calcium oxalate crystallization for the treatment of oxalate nephropathies. *Adv. Sci.* **7**, 1903337 (2020).
17. Trinchieri, A. et al. A prospective study of recurrence rate and risk factors for recurrence after a first renal stone. *J. Urol.* **162**, 27–30 (1999).
18. Neisius, A. et al. Shock wave lithotripsy: the new phoenix? *World J. Urol.* **33**, 213–221 (2015).
19. Sutherland, J. W., Parks, J. H. & Coe, F. L. Recurrence after a single renal stone in a community practice. *Miner. Electrolyte Metab.* **11**, 267–269 (1985).
20. Qaseem, A., Dallas, P., Forciea, M. A., Starkey, M. & Denberg, T. D. Clinical guidelines comm A. dietary and pharmacologic management to prevent recurrent nephrolithiasis in adults: a clinical practice guideline from the american college of physicians. *Ann. Intern. Med.* **161**, 659–685 (2014).
21. Shtukenberg, A. G., Ward, M. D. & Kahr, B. Crystal growth with macromolecular additives. *Chem. Rev.* **117**, 14042–14090 (2017).
22. Cho, K. R. et al. Mechanistic pathways for the molecular step growth of calcium oxalate monohydrate crystal revealed by in situ liquid-phase atomic force microscopy. *ACS Appl. Mater. Interfaces* **13**, 37873–37882 (2021).
23. Farmanesh, S., Alamani, B. G. & Rimer, J. D. Identifying alkali metal inhibitors of crystal growth: a selection criterion based on ion pair hydration energy. *Chem. Commun.* **51**, 13964–13967 (2015).
24. Alamani, B. G., Gale, J. D. & Rimer, J. D. Zinc ions modify calcium oxalate growth by distinct transformation of crystal surface termination. *Cryst. Growth Des.* **21**, 3375–3383 (2021).
25. Ozgurtas, T., Yakut, G., Gulec, M., Serdar, M. & Kutluay, T. Role of urinary zinc and copper on calcium oxalate stone formation. *Urol. Int.* **72**, 233–236 (2004).
26. Alamani, B. G. & Rimer, J. D. Molecular modifiers of kidney stones. *Curr. Opin. Nephrol. Hypertens.* **26**, 256–265 (2017).
27. Qiu, S. R. et al. Molecular modulation of calcium oxalate crystallization by osteopontin and citrate. *Proc. Natl Acad. Sci. USA* **101**, 1811–1815 (2004).
28. Ruiz-Agudo, E. et al. A non-classical view on calcium oxalate precipitation and the role of citrate. *Nat. Commun.* **8**, 1–10 (2017).
29. Li, S., Kang, X., He, Q., Tang, W. & Gong, J. Dual mechanism of natural polyphenols on crystal whiskers formation on calcium oxalate monohydrate crystal surface. *Appl. Surf. Sci.* **592**, 153355 (2022).
30. Jung, T. et al. Probing crystallization of calcium oxalate monohydrate and the role of macromolecule additives with in situ atomic force microscopy. *Langmuir* **20**, 8587–8596 (2004).
31. Wang, L. et al. Modulation of calcium oxalate crystallization by linear aspartic acid-rich peptides. *Langmuir* **22**, 7279–7285 (2006).
32. Olafson, K. N., Li, R., Alamani, B. G. & Rimer, J. D. Engineering crystal modifiers: bridging classical and nonclassical crystallization. *Chem. Mater.* **28**, 8453–8465 (2016).
33. Weaver, M. L. et al. Improved model for inhibition of pathological mineralization based on citrate-calcium oxalate monohydrate interaction. *Chemphyschem* **7**, 2081–2084 (2006).
34. Ortega, J. T. et al. Understanding severe acute respiratory syndrome coronavirus 2 replication to design efficient drug combination therapies. *Intervirology* **63**, 2–9 (2020).
35. Habtemariam, S. Recent advances in berberine inspired anticancer approaches: from drug combination to novel formulation technology and derivatization. *Molecules* **25**, 1426 (2020).
36. Van Nieuwenhuyse, B. et al. Bacteriophage-antibiotic combination therapy against extensively drug-resistant Pseudomonas aeruginosa infection to allow liver transplantation in a toddler. *Nat. Commun.* **13**, 5725 (2022).
37. Ma, W., Lutsko, J. F., Rimer, J. D. & Vekilov, P. G. Antagonistic cooperativity between crystal growth modifiers. *Nature* **577**, 497–501 (2020).
38. Tallarida, R. J. An overview of drug combination analysis with isobolograms. *J. Pharmacol. Exp. Ther.* **319**, 1–7 (2006).
39. Farmanesh, S. et al. Specificity of growth inhibitors and their cooperative effects in calcium oxalate monohydrate crystallization. *J. Am. Chem. Soc.* **136**, 367–376 (2014).
40. Lemann, J. et al. Urinary oxalate excretion increases with body size and decreases with increasing dietary calcium intake among healthy adults. *Kidney Int.* **49**, 200–208 (1996).
41. Chou, T. C. Theoretical basis, experimental design, and computerized simulation of synergism and antagonism in drug combination studies. *Pharmacol. Rev.* **58**, 621–681 (2006).
42. Chakrabarti, R. & Vekilov, P. G. Dual mode of action of organic crystal growth inhibitors. *Cryst. Growth Des.* **21**, 7053–7064 (2021).
43. Jones, F. & Ogden, M. I. Controlling crystal growth with modifiers. *CrystEngComm* **12**, 1016–1023 (2010).
44. Zhang, B. et al. Insights into ice-growth inhibition by trehalose and alginate oligosaccharides in peeled Pacific white shrimp (Litopenaeus vannamei) during frozen storage. *Food Chem.* **278**, 482–490 (2019).
45. Tang, W. et al. Tautomerism unveils a self-inhibition mechanism of crystallization. *Nat. Commun.* **14**, 561 (2023).
46. Sheng, X. X., Jung, T. S., Wesson, J. A. & Ward, M. D. Adhesion at calcium oxalate crystal surfaces and the effect of urinary constituents. *Proc. Natl Acad. Sci. USA* **102**, 267–272 (2005).
47. Lieske, J. C., Leonard, R. & Toback, F. G. Adhesion of calcium-oxalate monohydrate crystals to renal epithelial-cells is inhibited by specific anions. *Am. J. Physiol. Renal Fluid Electrolyte Physiol.* **268**, F604–F612 (1995).
48. Asselman, M., Verhulst, A., de Broe, M. E. & Verkoelen, C. F. Calcium oxalate crystal adherence to hyaluronan-, osteopontin-, and CD44-expressing injured/regenerating tubular epithelial cells in rat kidneys. *J. Am. Soc. Nephrol.* **14**, 3155–3166 (2003).
49. Mulay, S. R. & Anders, H. J. Crystal nephropathies: mechanisms of crystal-induced kidney injury. *Nat. Rev. Nephrol.* **13**, 226–240 (2017).
50. Herzog, R. et al. Lithium preserves peritoneal membrane integrity by suppressing mesothelial cell alpha B-crystallin. *Sci. Transl. Med.* **13**, eaaz9705 (2021).
51. Sun, X. Y., Zhang, C. Y., Bhadja, P. & Ouyang, J. M. Preparation, properties, formation mechanisms, and cytotoxicity of calcium oxalate monohydrate with various morphologies. *CrystEngComm* **20**, 75–87 (2018).

52. Okada, A. et al. Successful formation of calcium oxalate crystal deposition in mouse kidney by intraabdominal glyoxylate injection. *Urol. Res.* **35**, 89–99 (2007).
53. Shahrzad, S., Aoyagi, K., Winter, A., Koyama, A. & Bitsch, I. Pharmacokinetics of gallic acid and its relative bioavailability from tea in healthy humans. *J. Nutr.* **131**, 1207–1210 (2001).
54. Besenhofer, L. M., Cain, M. C., Dunning, C. & McMartin, K. E. Aluminum citrate prevents renal injury from calcium oxalate crystal deposition. *J. Am. Soc. Nephrol.* **23**, 2024–2033 (2012).
55. Mulay, S. R. et al. Hyperoxaluria requires TNF receptors to initiate crystal adhesion and kidney stone disease. *J. Am. Soc. Nephrol.* **28**, 761–768 (2017).
56. Zheng, J. et al. Protocatechuic acid from chicory is bioavailable and undergoes partial glucuronidation and sulfation in healthy humans. *Food Sci. Nutr.* **7**, 3071–3080 (2019).
57. Landete, J. M. Ellagitannins, ellagic acid and their derived metabolites: A review about source, metabolism, functions and health. *Food Res. Int.* **44**, 1150–1160 (2011).
58. Nakamura, Y., Tsuji, S. & Tonogai, Y. Method for analysis of tannic acid and its metabolites in biological samples: application to tannic acid metabolism in the rat. *J. Agric. Food Chem.* **51**, 331–339 (2003).
59. Del Valle, E. E., Spivacow, F. R. & Negri, A. L. Citrate and renal stones. *Medicina* **73**, 363–368 (2013).
60. Barcelo, P., Wuhl, O., Servitge, E., Rousaud, A. & Pak, C. Y. Randomized double-blind study of potassium citrate in idiopathic hypocitraturic calcium nephrolithiasis. *J. Urol.* **150**, 1761–1764 (1993).
61. Zhou, D. et al. Gallic acid ameliorates calcium oxalate crystal-induced renal injury via upregulation of Nrf2/HO-1 in the mouse model of stone formation. *Phytomedicine* **106**, 154429 (2022).

Acknowledgements

The authors are grateful for the financial support of the National Natural Science Foundation of China (NNSFC 22278300, 21808159, and 22078234) and the Natural Science Foundation of Tianjin (22JCZDJC00040).

Author contributions

S.L. and W.T. designed and planned the experiments. S.L. carried out bulk crystal growth studies, in situ AFM measurements, and theoretical modeling. D.H.Z. performed cell and animal experiments. Z.X.Z. completed batch bulk crystallization. S.L., W.T., X.Y.T., and J.B.G. analyzed the experimental data and wrote the manuscript.

Competing interests

The authors declare no competing interests.

Additional information

Supplementary information The online version contains supplementary material available at https://doi.org/10.1038/s43246-023-00393-0.

Correspondence and requests for materials should be addressed to Weiwei Tang or Junbo Gong.

Peer review information *Communications Materials* thanks the anonymous reviewers for their contribution to the peer review of this work. Primary Handling Editors: Jet-Sing Lee and John Plummer. A peer review file is available